IONIC TRANSPORT IN A CONTINUOUS DONNAN DIALYZER WITH A PARALLEL PLATE CHANNEL AND AN AGITATED TANK

KAZUHISA SATO, CHOUJI FUKUHARA,
TOSHIKUNI YONEMOTO AND TEIRIKI TADAKI
Department of Biochemistry and Engineering, Tohoku University, Sendai 980

Key Words: Ion Exchange Membrane, Mass Transfer, Membrane Separation, Numerical Simulation, Donnan Dialysis

Ionic transport in a continuous Donnan dialyzer with a parallel-plate channel and an agitated tank was studied for a bi-ionic exchange system. A theoretical model of the system was formulated on the basis of diffusion equations in terms of diffusion, migration and convection of each ion. Theoretical solutions were obtained by numerical calculations using a finite-difference technique. Simultaneously, continuous Donnan dialytic experiments were conducted for the K^+-H^+ exchange system with a cation-exchange membrane. The validity of this model was confirmed by comparison with experimental results for mean dialytic rates. The numerical calculation also provided distributions of ionic concentrations and the electric potential in the parallel-plate channel. An effectiveness factor was introduced to discuss the proportion of the mass transfer resistance in the membrane phase to the overall mass transfer resistance. The influence of Reynolds number and channel height on the mean dialytic rates and the effectiveness factor was also examined.

Introduction

Donnan dialysis[3,6-13,15-19] is an ionic separation method in which ions move across an ion-exchange membrane based on Donnan equilibrium.[1] Donnan dialytic apparatus is simple compared with that for electrodialysis which requires an electric field input. Therefore, applications of Donnan dialysis are expected to facilitate water softening,[19] recovery of metal ions from waste water[13] and deionization of a mixed solution of electrolytes and nonelectrolytes.[9] Dialyzers of the parallel-plate channel type with small gaps were usually used in previous studies. This is because a larger ratio of membrane effective area to dialyzer volume was desired.

It is essential to include not only diffusive but also migratory transport in the ion-exchange membrane. For the solution phase, a convective transport must be added to these two mechanisms. Therefore, the ionic transport process in the whole Donnan dialyzer is considerably complex, so few theoretical analyses[2,3,10] have been carried out.

In this paper, we deal with an ionic transport process in which bi-ionic exchange occurs between the solutions flowing in a parallel-plate channel and in an agitated tank across the ion-exchange membrane. The choice of such a system simplifies the theoretical analysis because ionic transport resistance in the agitated tank is negligible. A theoretical model of the system is formulated on the basis of diffusion equations in terms of diffusion, migration and convection. The influence of some factors on the dialytic rate is also discussed, with a comparison between numerical solutions of the model and experimental results.

Received July 5, 1990. Correspondence concerning this article should be addressed to T. Tadaki. C. Fukuhara is now at Dept. of Chem. Eng. Kogakuin University, Tokyo 160.

1. Theory

1.1 Model formulation

Consider a continuous ion-exchange system such as that shown in **Fig. 1**. A cation-exchange membrane separates the parallel-plate channel from the agitated tank. KCl and HCl aqueous solutions continuously flow in the channel and the tank respectively. The ion exchange of K^+ and H^+ occurs across the membrane. Ionic species K^+, H^+ and Cl^-, exist in the aqueous solutions. It is assumed that fully developed laminar flow in the channel and perfect agitation sufficient to ignore the solid-liquid mass transfer resistance in the tank are attained.

First, let us consider the membrane-phase mass transport. If no co-ion, Cl^-, exists in the membrane and if counter-ions, K^+ and H^+, move only in the y direction, the mass flux of each ion in the membrane is represented by the Nernst-Planck equation, as follows:

$$\bar{N}_i = -\bar{D}_i\left(\frac{d\bar{C}_i}{dy} + \bar{C}_i\frac{n_iF}{RT}\cdot\frac{d\bar{\phi}}{dy}\right) \quad (i=1,2) \tag{1}$$

$$\bar{N}_3 = 0 \tag{2}$$

where subscripts $i=1, 2$ and 3 refer to K^+, H^+ and Cl^- respectively. Integrating Eq. (1) gives the following equation[15]:

$$\bar{N}_1 = -\frac{1}{\delta_M}\cdot\frac{\bar{D}_1\bar{D}_2}{\bar{D}_1n_1-\bar{D}_2n_2}\left[(n_1-n_2)(\bar{C}_{1,C}-\bar{C}_{1,T}) - \frac{n_2n_FQ(\bar{D}_1-\bar{D}_2)}{\bar{D}_1n_1-\bar{D}_2n_2} \times \ln\left\{\frac{n_1(\bar{D}_1n_1-\bar{D}_2n_2)\bar{C}_{1,C}-\bar{D}_2n_2Qn_F}{n_1(\bar{D}_1n_1-\bar{D}_2n_2)\bar{C}_{1,T}-\bar{D}_2n_2Qn_F}\right\}\right] \tag{3}$$

$$\bar{N}_2 = -\frac{n_1}{n_2}\bar{N}_1$$

Next, consider the solution-phase mass transport in the channel. It is assumed that diffusive and migratory transport in the x direction is negligibly small compared with convective transport. The diffusion equation of each ion is

$$u\frac{\partial C_i}{\partial x} - D_i\frac{\partial}{\partial y}\left\{\frac{\partial c_i}{\partial y} + \frac{n_iC_iF}{RT}\cdot\frac{\partial\phi}{\partial y}\right\} = 0 \quad (i=1,2,3) \tag{4}$$

where the term in brackets multiplied by $-D_i$ represents the ionic flux in the direction of y axis, N_i. The electroneutrality condition is

$$\sum_{i=1}^{3} n_iC_i = 0 \tag{5}$$

Eliminating the term of the electric potential gradient from Eq. (4) using Eq. (5) (see **Appendix 1**) gives

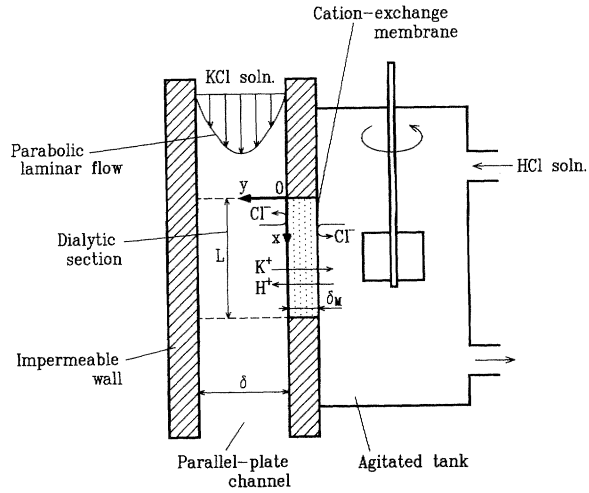

Fig. 1. Schematic diagram of ionic transport process in continuous Donnan dialyzer

$$u\frac{\partial C_i}{\partial x} - D_i\frac{\partial^2 C_i}{\partial y^2} + D_in_i\frac{\partial}{\partial y}\left\{C_i\frac{\sum_{\eta}^{3} D_\eta n_\eta(\partial C_\eta/\partial y)}{\sum_{\eta}^{3} D_\eta n_\eta^2 C_\eta}\right\} = 0 \tag{6}$$

Multiplying Eq. (6) by $\delta/(6\bar{u}Q)$ and introducing dimensionless numbers gives

$$U\frac{\partial Z_i}{\partial X} - S_i\frac{\partial^2 Z_i}{\partial Y^2} + S_in_i\frac{\partial}{\partial Y}\left\{Z_i\frac{\sum_{\eta}^{3} S_\eta n_\eta(\partial Z_\eta/\partial Y)}{\sum_{\eta}^{3} S_\eta n_\eta^2 Z_\eta}\right\} = 0 \tag{7}$$

where dimensionless velocity, U, is given as

$$U = Y - Y^2 \tag{8}$$

Initial conditions at an inlet of the channel are

$$X=0, \quad Z_i = Z_{i,C}|_{in} \quad (i=1,2,3) \tag{9}$$

At the membrane-solution interface on the channel side, $Y=0$, the dimensionless flux of the membrane phase is equal to that of liquid phase, and the equilibrium relation holds so that

$$Y=0; \quad \mathcal{N}_i = \bar{\mathcal{N}}_i \quad (i=1,2), \qquad \mathcal{N}_3 = 0 \tag{10}$$

$$K_2^1 = \frac{\bar{C}_1^{|n_2|}\cdot C_2^{|n_1|}}{C_1^{|n_2|}\cdot\bar{C}_2^{|n_1|}} = \frac{\bar{C}_1^{|n_2|}\cdot Z_2^{|n_1|}}{Z_1^{|n_2|}\cdot\bar{C}_2^{|n_1|}}Q^{|n_1|-|n_2|} \tag{11}$$

where K_2^1 is the selectivity coefficient.[5]

The boundary condition at the impermeable wall, $Y=1$, is

$$Y=1; \quad \mathcal{N}_i = 0 \quad (i=1,2,3) \tag{12}$$

On the other hand, at the membrane-solution

interface on the agitated-tank side, $Y=-\delta_M/\delta$, the boundary condition is

$$Y=-\delta_M/\delta;$$

$$K_2^1=\frac{\bar{C}_1^{|n_2|}\cdot C_{2,T}^{|n_1|}}{C_{1,T}^{|n_2|}\cdot \bar{C}_2^{|n_1|}}=\frac{\bar{C}_1^{|n_2|}\cdot Z_{2,T}^{|n_1|}}{Z_{1,T}^{|n_2|}\cdot \bar{C}_2^{|n_1|}}Q^{|n_1|-|n_2|} \tag{13}$$

The dimensionless concentration on the tank side, $Z_{i,T}$, must satisfy the following mass balance equation:

$$Z_{i,T}=Z_{i,T}|_{out}=(Z_{i,C}|_{in}-Z_{i,C}|_{out})\frac{V_C}{V_T}+Z_{i,T}|_{in} \tag{14}$$

1.2 Numerical calculation

Equation (7) was finite-differentiated by using backward-difference approximations for $\partial/\partial X$ and central-difference approximations for $\partial/\partial Y$ and $\partial^2/\partial Y^2$. **Figure 2** shows the grid system used to set up the formulation.

For a given node, except at $k=1$ and $k=KT$, the following equation is obtained by the finite-differentiation of Eq. (7):

$$V_k\frac{Z_{i,j,k}-Z_{i,j-1,k}}{\Delta X}-S_i\frac{Z_{i,j,k+1}-2Z_{i,j,k}+Z_{i,j,k-1}}{\Delta Y}$$

$$+\frac{S_in_i}{\Delta Y}\left\{\frac{(Z_{i,j,k+1}+Z_{i,j,k})\sum_\eta^3\{S_\eta n_\eta(Z_{\eta,j,k+1}-Z_{\eta,j,k})\}}{\sum_\eta^3\{S_\eta n_\eta^2(Z_{\eta,j,k+1}Z_{\eta,j,k})\}}\right.$$

$$\left.-\frac{(Z_{i,j,k}+Z_{i,j,k-1})\sum_\eta^3\{S_\eta n_\eta(Z_{\eta,j,k}-Z_{\eta,j,k-1})\}}{\sum_\eta^3\{S_\eta n_\eta^2(Z_{\eta,j,k}+Z_{\eta,j,k-1})\}}\right\}=0$$

$$(i=1,2,3\quad k=2\sim KT-1) \tag{15}$$

For a node at $k=1$, i.e. at the membrane-solution interface, the finite-differentiation of Eq. (7) with Eq. (10) (see **Appendix 2**) gives

$$\frac{V_1}{4}\cdot\frac{3Z_{i,j,1}+Z_{i,j,2}-3Z_{i,j-1,1}-Z_{i,j-1,2}}{\Delta X}$$

$$-S_i\frac{Z_{i,j,2}-Z_{i,j,1}}{\Delta Y}$$

$$+\frac{S_in_i}{\Delta Y}\cdot\frac{(Z_{i,j,2}+Z_{i,j,1})\sum_\eta^3\{S_\eta n_\eta(Z_{\eta,j,2}-Z_{\eta,j,1})\}}{\sum_\eta^3\{S_\eta n_\eta^2(Z_{\eta,j,2}+Z_{\eta,j,1})\}}$$

$$-\mathcal{N}_i|_{Y=0}=0\quad(i=1,2,3) \tag{16}$$

On the other hand, for a node at $k=KT$, i.e. at the impermeable wall, the finite-differentiation of Eq. (7) with Eq. (12) gives:

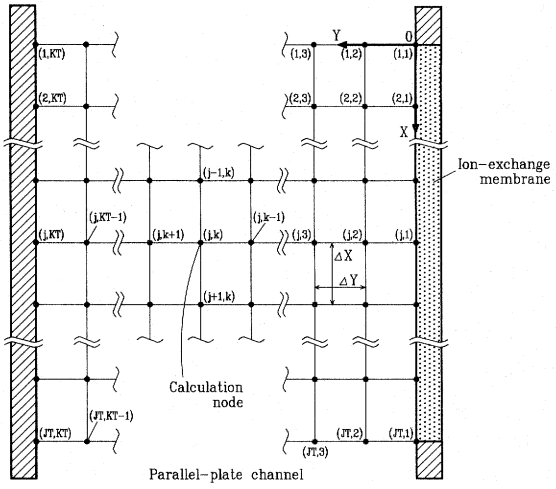

Fig. 2. Finite-difference grid system

$$\frac{V_{KT}}{4}\cdot\frac{3Z_{i,j,KT}+Z_{i,j,KT-1}-3Z_{i,j-1,KT}-Z_{i,j-1,KT-1}}{\Delta X}$$

$$+S_i\frac{Z_{i,j,KT}-Z_{i,j,KT-1}}{\Delta Y}-\frac{S_in_i}{\Delta Y}$$

$$\times\frac{(Z_{i,j,KT}+Z_{i,j,KT-1})\sum_\eta^3\{S_\eta n_\eta(Z_{\eta,j,KT}-Z_{\eta,j,KT-1})\}}{\sum_\eta^3\{S_\eta n_\eta^2(Z_{\eta,j,KT}+Z_{\eta,j,KT-1})\}}$$

$$=0\quad(i=1,2,3) \tag{17}$$

The volumetric flow rates in Eqs. (15) to (17), V_k, are

$$V_k=\int_{Y-\Delta Y/2}^{Y+\Delta Y/2}U\cdot dY=U(Y)\Delta Y-\frac{\Delta Y^3}{12}$$

$$(k=2\sim KT-1)$$

$$\int_0^{\Delta Y/2}U\cdot dY=\int_{1-\Delta Y/2}^1U\cdot dY=\left(1-\frac{\Delta Y}{3}\right)\frac{\Delta Y^2}{8} \tag{18}$$

$$(k=1,\ KT)$$

Equation (3) and Eqs. (15) to (17) were solved by the Newton-Raphson iterative technique under restrictions (9) to (14). The ionic concentration in the tank, $Z_{i,T}$, is unknown at the start of the first calculation. Therefore, the numerical calculation was first done by using an assumed appropriate value of $Z_{i,T}$, and the mixing cap average concentration at the channel outlet was obtained as follows:

$$Z_{i,C}|_{out}=\frac{\int_0^1 Z_i|_{X=L/\delta}U\cdot dY}{\int_0^1 U\cdot dY} \tag{19}$$

Next, $Z_{i,T}$ was renewed by substituting $Z_{i,C}|_{out}$ to Eq. (14). Then, the same procedure was repeated until $Z_{i,T}$

converged.

2. Experimental

2.1 Apparatus and procedure

The dialyzer consisted of a cation-exchange membrane, an agitated tank and an end-plate made of acrylic resin, as shown in **Fig. 3**. The cation-exchange membrane was Neosepta CM-1, made by Tokuyama Soda Co., Ltd. The membrane was fastened between the end-plate and the agitated tank with silicone rubber gaskets. The parallel-plate channel between the membrane and the end-plate was 1.8×10^{-3} m in height (δ) and 3.00×10^{-2} m in width (W). The surface of the membrane was coated with polyvinyl chloride film excepted for a dialytic section of 5.00×10^{-2} m in length, L, in the middle of the membrane so that no chemical species could permeate through its coated area. The effective area of permeation, A, therefore, was 1.50×10^{-3} m^2.

An aqueous solution of 100 mol·m^{-3} KCl was fed continuously into the channel at $Re=5\sim100$, and 100 mol·m^{-3} HCl aqueous solution was also fed continuously into the tank at the same volumetric flow rate as into the channel. An impeller in the tank was rotated at 1500 rpm. The rotation speed was sufficiently high to ignore the mass transfer resistance in the liquid phase of the tank.

After steady state was attained, the solutions leaving the channel and the tank were sampled. The concentration of H^+ in the sample was determined by neutralization titration with NaOH solution in nitrogen atmosphere. The concentration of K^+ was determined by an ion chromatograph IC-200 (Yokogawa Electric Co., Ltd.).

Experiments were conducted at 298 ± 0.5 K by using a temperature-controlled water bath.

2.2 Physical properties

Physical properties used in the numerical calculations are listed in **Table 1**. The ionic diffusion coefficients in the aqueous solution were estimated from its limiting equivalent conductivities.[4,14] The membrane thickness, the ion-exchange capacity, the selectivity coefficient and the ionic diffusion coefficients in the membrane were measured experimentally.[15]

3. Results and Discussion

The effect of the number of grid points on computational accuracy was first investigated. The dimensionless integral of ionic permeation rates across the membrane

$$\xi_{F,i}=\int_0^{L/\delta}\bar{\mathcal{N}}_i dX \tag{20}$$

and the dimensionless increments in ionic mass flow rate at the outlet of the channel

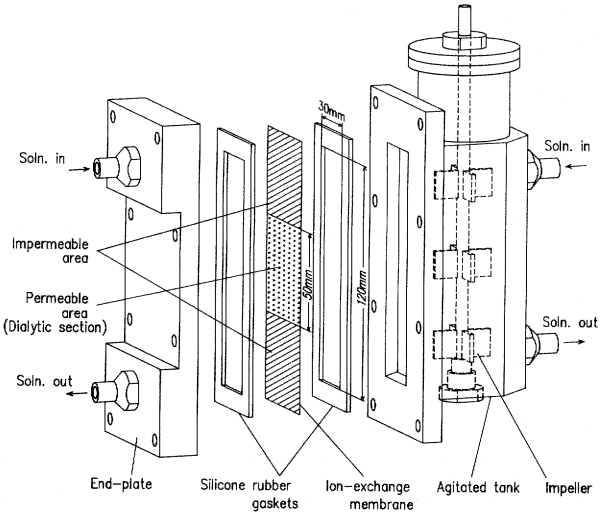

Fig. 3. Detail drawing of continuous Donnan dialyzer

Table 1. Physical properties and other parameters used in numerical calculation

for solution phase:	
Diffusion coefficients, D_i	
$i=K^+$	1.95×10^{-9} m^2·s^{-1}
H^+	9.31×10^{-9} m^2·s^{-1}
Cl^-	2.03×10^{-9} m^2·s^{-1}
Kinematic viscosity, ν	8.97×10^{-7} m^2·s^{-1}
for cation-exchange membrane:	
Thickness, δ_M	1.44×10^{-4} m
Ion exchange capacity, Q	2.10×10^{3} mol·m^{-3}
Valency of fixed ion, n_F	-1
Diffusion coefficients, $\bar{D}_i$	
$i=K^+$	1.35×10^{-10} m^2·s^{-1}
H^+	4.80×10^{-10} m^2·s^{-1}
Selectivity coefficient*	$\ln K_H^K=1.11-1.06X_K$
Dimensions of parallel-plate channel:	
Length of dialytic section, L	5.00×10^{-2} m
Width of channel, W	3.00×10^{-2} m

* $K_H^K=\dfrac{\bar{C}_K\cdot C_H}{C_K\cdot\bar{C}_H}$, $X_K=\dfrac{C_K}{C_K+C_H}$

$$\xi_{M,i}=\int_0^1 (Z_i|_{X=L/\delta}-Z_{i,C}|_{in})U\cdot dY \tag{21}$$

were calculated for different numbers of grid points in the X and Y directions. Overall mass balance requires that

$$\xi_{F,i}=\xi_{M,i} \tag{22}$$

Table 2 shows that the calculation results are almost the same when the grid point numbers increase or decrease around $JT\times KT=501\times101$, and that Eq. (22) is almost satisfied. Subsequent calculations, therefore, were performed with these grid point numbers.

The theoretical mean dialytic rates of K^+ and H^+, $\mathcal{M}_i$,

Table 2. Mass balance of numerical calculation ($Re=10.0$, $\delta=1.8\times10^{-3}$ m)

$JT\times KT$	ξ_{F,H^+} [—]	ξ_{M,H^+} [—]
251×51	3.814×10^{-4}	3.810×10^{-4}
251×101	3.812×10^{-4}	3.811×10^{-4}
501×51	3.815×10^{-4}	3.811×10^{-4}
501×101	3.814×10^{-4}	3.812×10^{-4}
501×201	3.811×10^{-4}	3.814×10^{-4}
1001×101	3.814×10^{-4}	3.813×10^{-4}
1001×201	3.812×10^{-4}	3.814×10^{-4}

$$\mathscr{M}_i=\left|\frac{(C_{i,C}|_{out}-C_{i,C}|_{in})\cdot\bar{u}\cdot\delta\cdot W}{A}\right| \qquad (23)$$

for various heights of the channel, δ, are shown with experimental data in **Fig. 4.** $\mathscr{M}_{K^+}$ and $\mathscr{M}_{H^+}$ are equal because the local fluxes of these two ionic species in the membrane have equal absolute values and opposite signs, as shown in Eq. (3). First, it can be seen from the figure that theoretical $\mathscr{M}_i$ increases with Re and decreases with δ. Next, the measured $\mathscr{M}_{K^+}$ and $\mathscr{M}_{H^+}$ are almost equal, so the experimental mass balance is also satisfied. The experimental data agree with the calculated line for $\delta=1.8$ mm at any Re number. The model formulation and the calculation procedure, therefore, were considered to be appropriate.

Figure 5 shows theoretical iso-concentration lines in the channel. A concentration boundary layer is formed at the membrane-liquid interface from the starting point of the dialytic section. Figure 5 (c) shows that the concentration of the co-ion, i.e. Cl^-, is not uniform in the channel even though the ion does not permeate the membrane.

Figure 6 shows distributions of the ionic concentrations and the electric potential in the direction of the Y axis (see **Appendix 3**). Ionic concentration gradients increase with Re in both the channel and the membrane. This phenomenon corresponds to the increase of $\mathscr{M}_i$ with Re in Fig. 4. The dimensionless electric potential, Φ, increases in the Y direction. The potential gradient forms for the following reason. K^+ and H^+ diffuse in the counterdirection along the Y axis in the channel, but these two ionic species differ from each other in mobility; that is, the potential increases in the direction in which H^+, which has larger mobility, diffuses. The chloride ion migrates away from the membrane due to the potential gradient so that its concentration is not uniform in the channel, as shown in Fig. 5 (c).

Next, an effectiveness factor η is introduced to investigate the proportion of the mass transfer resistance in the membrane phase to the overall mass transfer resistance:

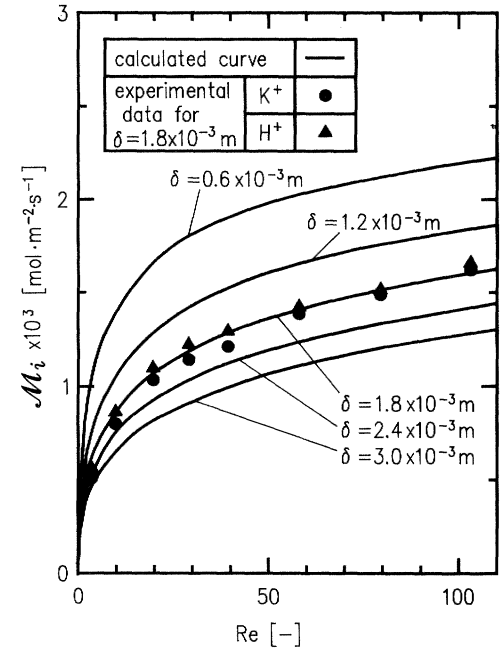

Fig. 4. Theoretical and experimental mean dialytic rates

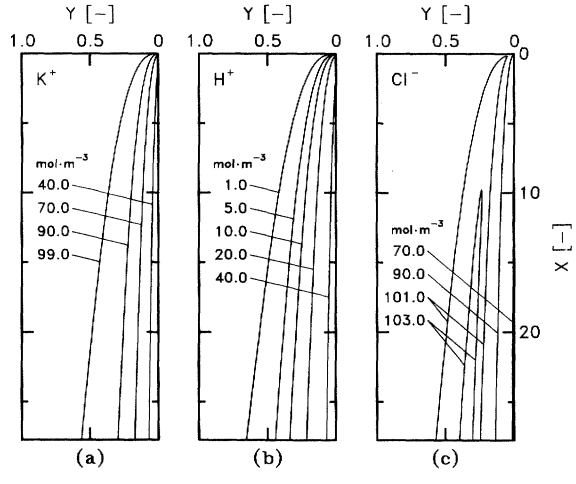

Fig. 5. Theoretical contours of ionic concentration in parallel-plate channel. ($Re=5.0$, $\delta=1.8\times10^{-3}$ m)

$$\eta=\frac{(\mathscr{M}_i \text{ calculated considering mass transfer resistance of liquid phase in the channel})}{(\mathscr{M}_i \text{ calculated ignoring mass transfer resistance of liquid phase in the channel})} \qquad (24)$$

The denominator of Eq. (24) is the mean dialytic rate, which is calculated by assuming the concentration in the channel to be constant in the direction of the Y axis. The effectiveness factor, η, has a value between 0 and 1; η approaches 0 in the case where the mass transfer in the liquid phase is rate-controlling, and it approaches 1 in the case where the membrane transport is rate-controlling.

Figure 7 shows the calculated η values. It can be seen that η increases as the channel height, δ, decreases so that dialysis becomes more effective as δ becomes

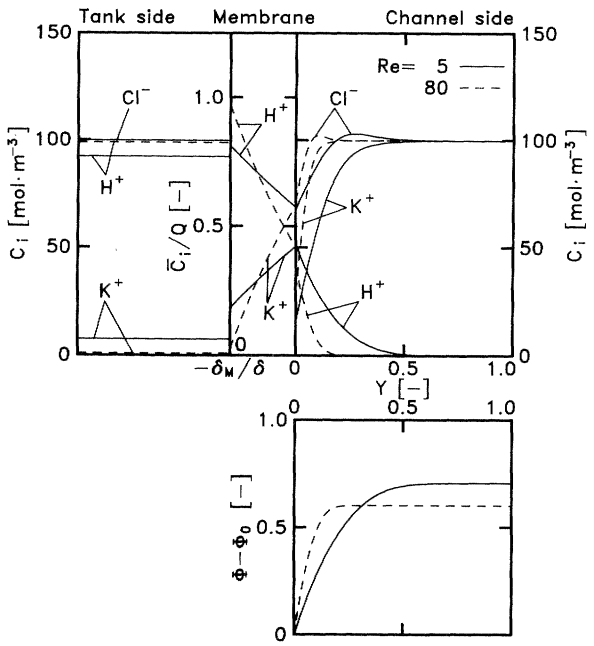

Fig. 6. Theoretical distributions of ionic concentration and electric potential along the Y axis. ($X=13.9$, $\delta=1.8\times10^{-3}$ m)

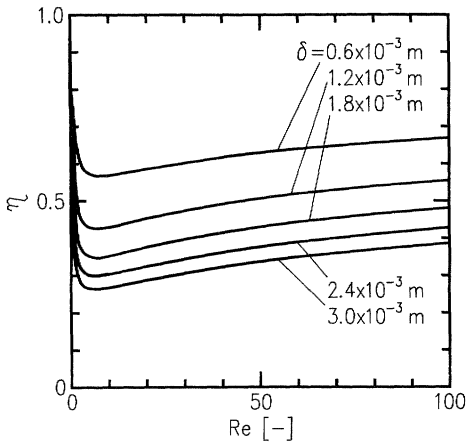

Fig. 7. Theoretical effectiveness factor

smaller. Additionally, η takes a minimum value at about $Re=5$ for any δ. In the region of $Re>5$, η increases with Re. This is because the mass transfer resistance in the liquid decreases with increasing Re. In the region of $Re<5$, however, η becomes close to unity as Re approaches 0 because the concentration profile along the Y axis in the channel becomes flat as the Re number decreases. The value of η becomes 0.35 to 0.48 for $\delta=1.8$ mm in the range of $Re=5\sim100$ in which the study was carried out, as shown in Fig. 7. Therefore, it is considered that the contributions of mass transfer resistance in the membrane and in the liquid phase are roughly comparable.

Conclusion

Ionic transport in the continuous Donnan dialyzer with parallel-plate channel and the agitated tank was modeled based on the diffusion equations, and the theoretical solutions were obtained by numerical calculations. The validity of this the model was confirmed by comparison with experimental results for the mean dialytic rates. The numerical calculation provided not only the mean dialytic rates but also distributions of the ionic concentrations and the electric potential in the parallel-plate channel. Additionally, the effectiveness factor, η, was introduced to examine the proportion of mass transfer resistance in the membrane phase to the overall mass transfer resistance, and the influence of Re and the channel height, δ, on η was revealed.

Appendix 1

Multiplying Eq. (4) by n_i and summing with respect to i yields

$$u\frac{\partial\sum_i^3 n_iC_i}{\partial x}-\frac{\partial}{\partial y}\left\{\sum_i^3 n_iD_i\left(\frac{\partial C_i}{\partial y}+\frac{n_iC_iF}{RT}\cdot\frac{\partial\phi}{\partial y}\right)\right\}=0 \tag{A-1}$$

Eliminating the first term in Eq. (A-1) by using Eq. (5) gives

$$\sum_i^3 n_iD_i\left(\frac{\partial C_i}{\partial y}+\frac{n_iC_iF}{RT}\cdot\frac{\partial\phi}{\partial y}\right)=\text{constant}=I/F \tag{A-2}$$

where I is an electric current. At the impermeable wall, $y=\delta$, no electric current flows ($I=0$) so the following equation is obtained:

$$\frac{F}{RT}\cdot\frac{\partial\phi}{\partial y}=-\frac{\sum_i^3 D_in_i(\partial C_i/\partial y)}{\sum_i^3 D_in_i^2C_i} \tag{A-3}$$

Appendix 2

Finite-differentiating Eq. (7) at $k=1$ yields

$$V_1\frac{\tilde{Z}_{i,j}-\tilde{Z}_{i,j-1}}{\Delta X}-S_i\frac{Z_{i,j,2}-Z_{i,j,1}}{\Delta Y}$$
$$+\frac{S_in_i}{\Delta Y}\cdot\frac{(Z_{i,j,2}+Z_{i,j,1})\sum_\eta^3\{S_\eta n_\eta(Z_{\eta,j,2}-Z_{\eta,j,1})\}}{\sum_\eta^3\{S_\eta n_\eta^2(Z_{\eta,j,2}+Z_{\eta,j,1})\}}$$
$$-\mathcal{N}_i|_{Y=0}=0\quad(i=1,2,3) \tag{A-4}$$

where $\tilde{Z}$ is an average concentration between $Y=0$ and $Y=\Delta Y/2$. Assuming that the concentration distribution along the Y axis is linear in the region of $Y=0\sim\Delta Y$ gives

$$\tilde{Z}_{i,j}=\frac{3Z_{i,j,1}+Z_{i,j,2}}{4}$$
$$\tilde{Z}_{i,j-1}=\frac{3Z_{i,j-1,1}+Z_{i,j-1,2}}{4} \tag{A-5}$$

Substitution of Eq. (A-5) into Eq. (A-4) yields Eq. (16). Equation (17) is obtained in the same way.

Appendix 3

The following equation is obtained from Eq. (3):

$$\bar{N}_1(y+\delta_M)+\frac{\bar{D}_1\bar{D}_2}{\bar{D}_1n_1-\bar{D}_2n_2}\left[(n_1-n_2)(\bar{C}_1|_y-\bar{C}_{1,T})\right.$$
$$\left.-\frac{n_2n_FQ(\bar{D}_1-\bar{D}_2)}{\bar{D}_1n_1-\bar{D}_2n_2}\ln\left\{\frac{n_1(\bar{D}_1n_1-\bar{D}_2n_2)\bar{C}_1|_y-\bar{D}_2n_2Qn_F}{n_1(\bar{D}_1n_1-\bar{D}_2n_2)\bar{C}_{1,T}-\bar{D}_2n_2Qn_F}\right\}\right]=0 \tag{A-6}$$

The concentration distribution along the y axis can be obtained if Eq. (A-6) is solved in terms of $\bar{C}_1|_y$ for given y.

On the other hand, when considering the fixed x axis, Eq. (A-3) gives

$$d\Phi = -\frac{\sum_i^3 S_i n_i dZ_i}{\sum_i^3 S_i n_i^2 Z_i} \quad \text{B.C. } \Phi=\Phi_0 \text{ at } Y=0 \qquad \text{(A-7)}$$

The electric potential distribution along the y axis can be obtained by solving Eq. (A-7) numerically.

Nomenclature

A	=	effective area of membrane	[m^2]
C_i	=	ionic concentration	[$mol \cdot m^{-3}$]
D_i	=	ionic diffusion coefficient	[$m^2 \cdot s^{-1}$]
F	=	Faraday's constant	[$C \cdot mol^{-1}$]
K_2^1	=	selectivity coefficient	[—]
L	=	length of dialytic section in the x direction	[m]
$\mathscr{M}_i$	=	mean dialytic rate of ion i	[$mol \cdot m^{-2} \cdot s^{-1}$]
N_i	=	ionic flux in the direction of the y axis	[$mol \cdot m^{-2} \cdot s^{-1}$]
$\mathscr{N}_i$	=	dimensionless ionic flux, $N_i/6\bar{u}Q$	[—]
n_i	=	valence	[—]
Q	=	concentration of fixed ion (ion exchange capacity)	[$mol \cdot m^{-3}$]
R	=	gas constant	[$J \cdot mol^{-1} \cdot K^{-1}$]
Re	=	Reynolds number, $\delta\bar{u}/\nu$	[—]
S_i	=	dimensionless ionic diffusion coefficient, $D_i/6\bar{u}\delta$	[—]
T	=	temperature	[K]
U	=	dimensionless velocity, $u/6\bar{u}$	[—]
u	=	velocity in parallel-plate channel	[$m \cdot s^{-1}$]
$\bar{u}$	=	average velocity in parallel-plate channel	[$m \cdot s^{-1}$]
V	=	dimensionless volumetric flow rate in parallel-plate channel	[—]
W	=	width of parallel-plate channel	[m]
X	=	dimensionless x coordinate, x/δ	[—]
x	=	coordinate parallel to flow	[m]
Y	=	dimensionless y coordinate, y/δ	[—]
y	=	coordinate normal to flow	[m]
Z	=	dimensionless ionic concentration, C/Q	[—]
Δ	=	delta (difference) operator	
δ	=	height of parallel-plate channel	[m]
δ_M	=	thickness of membrane	[m]
η	=	effectiveness factor	[—]
ν	=	kinematic viscosity	[$m^2 \cdot s^{-1}$]
ξ_F	=	dimensionless integral of ionic permeation rate across membrane, defined by Eq. (20)	[—]
ξ_M	=	dimensionless increment in ionic mass flow rate at outlet of parallel-plate channel, defined by Eq. (21)	[—]
Φ	=	dimensionless electric potential, $F\phi/RT$	[—]
ϕ	=	electric potential	[V]

⟨Subscripts⟩

C	=	parallel-plate channel side
F	=	fixed ion in membrane
i	=	ionic species (1: K^+, 2: H^+, 3: Cl^-)
in	=	inlet of parallel-plate channel or agitated tank
JT	=	number of nodes in the X direction
j	=	grid point for the X axis
KT	=	number of nodes in the Y direction
k	=	grid point for the Y axis
out	=	outlet
T	=	agitated-tank side

⟨Superscripts⟩

—	=	in membrane phase
~	=	refers to average value defined by Eq. (A-5)

Literature Cited

1) Donnan, F. G.: *Chem. Rev.*, **1**, 73 (1924).
2) Helfferich, F.: *J. Phys. Chem.*, **66**, 39 (1962).
3) Helfferich, F.: *J. Phys. Chem.*, **67**, 1157 (1963).
4) Helfferich, F.: "Ion Exchange", p. 268, McGraw-Hill, New York (1962).
5) Helfferich, F.: "Ion Exchange", p. 153, McGraw-Hill, New York (1962).
6) Huang, T. C. and P. H. Lian: *Ind. Eng. Chem. Fundam.*, **18**, 221 (1979).
7) Huang, T. C.: *J. Chem. Eng. Japan*, **13**, 49 (1980).
8) Huang, T. C. and Y. K. Lin: *J. Chem. Eng. Japan*, **20**, 511 (1987).
9) Igawa, M., K. Echizenya, T. Hayashita and M. Seno: *Bull. Chem. Soc. Japan*, **60**, 381 (1987).
10) Inenaga, K. and N. Yoshida: *J. Membrane Sci.*, **6**, 271 (1980).
11) Kojima, T., S. Furusaki and K. Saito: *Can. J. Chem. Eng.*, **60**, 650 (1982).
12) Lake, M. A. and S. S. Melsheimer: *AIChE J.*, **24**, 130 (1978).
13) Ng, P. K. and D. D. Snyder: *J. Electrochem. Soc.*, **128**, 1714 (1981).
14) Robinson, R. A. and R. H. Stokes: "Electrolyte Solutions", 2nd ed., p. 317, Butterworths Pub., London (1959).
15) Sato, K., T. Yonemoto and T. Tadaki: *J. Membrane Sci.*, **53**, 215 (1990).
16) Sudoh, M., H. Kamei and S. Nakamura: *J. Chem. Eng. Japan*, **20**, 34 (1987).
17) Takahashi, K., K. Tsuboi and H. Takeuchi: *J. Chem. Eng. Japan*, **22**, 532 (1989).
18) Wallace, R. M.: *Ind. Eng. Chem. Process Des. Develop.*, **6**, 423 (1967).
19) Wendt, R. P.: *J. Membrane Sci.*, **1**, 165 (1976).